

Molecular structure and hydrolytic stability amidinium salts derived from triazatricyclo[5.2.1.0^{4,10}]decane

Andrew R. Battle and Leone Spiccia*

School of Chemistry, Monash University, Clayton, Vic. 3800, Australia

Received 14 February 2005; revised 3 May 2005; accepted 19 May 2005

Available online 15 June 2005

Abstract—Five amidinium salts have been prepared from triazatricyclo[5.2.1.0^{4,10}]decane (tacnoa) and characterised by mass spectrometry, NMR spectroscopy and X-ray crystallography. The X-ray structures revealed a long distance between the methine carbon and the ammonium nitrogen, viz., C–N distance 1.64–1.70 Å, cf. other C–N distances of 1.40–1.50 Å. An NMR study of 1-ethyl-4,7-diaza-1-azoniatricyclo[5.2.1.0^{4,10}]decane and 1-benzyl-4,7-diaza-1-azoniatricyclo[5.2.1.0^{4,10}]decane, confirmed that these amidinium salts hydrolyse in aqueous solution, the latter 60 times faster than the former. Tacnoa, which has C–N distances typical of single bonds, showed no evidence of hydrolysis after several days at 80 °C. Molecular modeling calculations indicate that the preferred gas phase structure of the salts is one where the positive charge is delocalised over the two secondary amines and the methine carbon. The calculated distance between this carbon and the ammonium nitrogen is 0.15–0.4 Å longer than in the crystal structure. The energy difference between the preferred gas phase and solid state conformations is 2 kJ mol⁻¹ and presents little barrier to nucleophilic attack of the methine carbon. Further analysis of the methine carbon geometry (C(7)) reveals that the bond angles in the benzyl salt are closer to those expected for an sp² centre than in the ethyl salt and that this could be the origin of the faster hydrolysis rate.

© 2005 Elsevier Ltd. All rights reserved.

1. Introduction

Triazatricyclo[5.2.1.0^{4,10}]decane, tacnorthoamide (tacnoa) has been extensively used as a synthon to N-substituted derivatives of 1,4,7-triazacyclononane (tacn).^{1–18} A reaction sequence summarising aspects of this efficient chemistry is shown in [Scheme 1](#). In aprotic solvents, tacnoa reacts readily with a variety of electrophiles forming amidinium salts, which are readily hydrolysed in water to give formyl derivatives. These formyl derivatives have a single secondary nitrogen at which further functionalisation can be achieved by reaction with a second electrophile. Hydrolysis of the formyl group in acid yields a di-substituted tacn derivative, which can be reacted with a third electrophile to yield the asymmetric tri-substituted tacn derivative.⁷

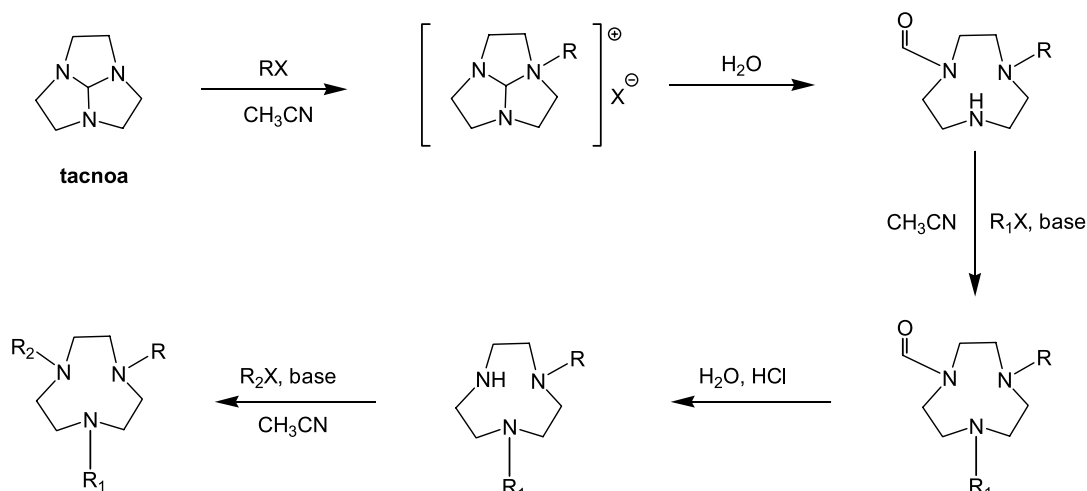
The tacnoa synthon has also proved extremely useful in the development of syntheses to ligands that incorporate two, three or four tacn macrocycles within the same framework.^{19–30} Reaction of bis-, tris- or tetrakis-electrophiles with tacnoa yields the corresponding bis-, tris- or tetrakis-

amidinium salts, which can be hydrolysed to ligands comprising two to four macrocycles held together by various aliphatic and aromatic groups. In principle, asymmetric poly(tacn) assemblies can also be prepared since, as was the case for the mono-amidinium salts, hydrolysis of the poly-amidinium salts gives poly-formyl derivatives that can be functionalised at each exposed secondary amine. Hydrolysis of the formyl groups generates derivatives in which each macrocycle is mono-functionalised and has a single secondary amine on which further functionalisation can be carried out.

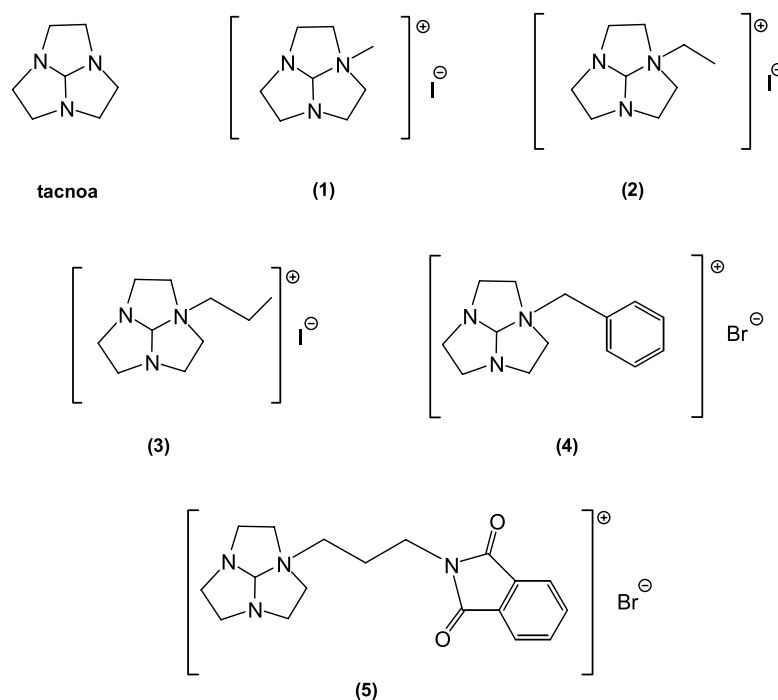
The synthetic utility of tacnoa and amidinium derivatives thereof has led us to explore the structure and hydrolytic stability of amidinium derivatives of tacnoa (such as **1–5** below). In particular, we report herein the X-ray crystal structure of four such amidinium salts (**2–5**), some of which have been reported by other workers^{4,7,31} but not subjected to X-ray structure determination, together with measurements of the rate of hydrolysis of two of these compounds. To aid in the elucidation of the origin of differences in hydrolytic reactivity, the X-ray structures have been complemented by molecular modeling calculations and measurements of the rate of hydrolysis, in neutral aqueous solution, on two amidinium salts and tacnoa.

Keywords: 1,4,7-Triazacyclononane; Amidinium salts; X-ray structure; Hydrolysis rate; Molecular modeling.

* Corresponding author. Tel.: +61 3 9905 4526; fax: +61 3 9905 4597; e-mail: leone.spiccia@sci.monash.edu.au



Scheme 1.



2. Results and discussion

All compounds were obtained as white microcrystalline solids in excellent yields ($\geq 90\%$). They gave clean ^1H and ^{13}C NMR spectra and ESI-MS signal at the appropriate m/z values. They are moderately stable to moisture but dissolve readily in H_2O , whereupon hydrolysis occurs. The rates of hydrolysis of two compounds, **2** and **4**, were found to differ (see below) but both were faster than the rate of hydrolysis of triazatricyclo[5.2.1.0^{4,10}]decane (tacnoa).

2.1. Description of structures

Details of crystal structure refinements are given in Table 1. A single X-ray crystal analysis confirmed the structure of **2** to consist of discrete tacnoa cations and iodide anions

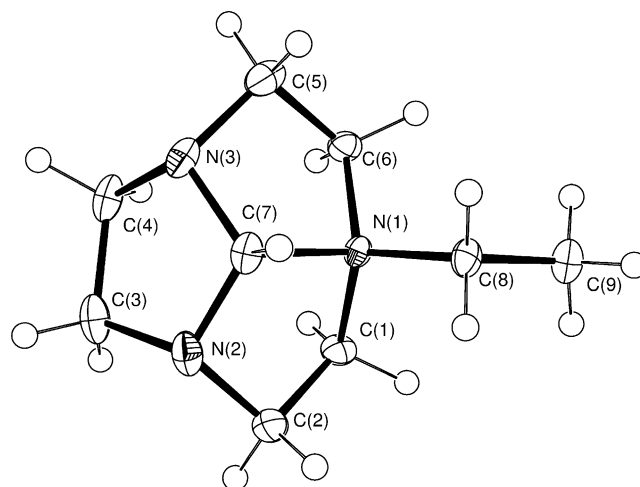


Figure 1. ORTEP representation of the cation in **2** (probability ellipsoids drawn at 50%).

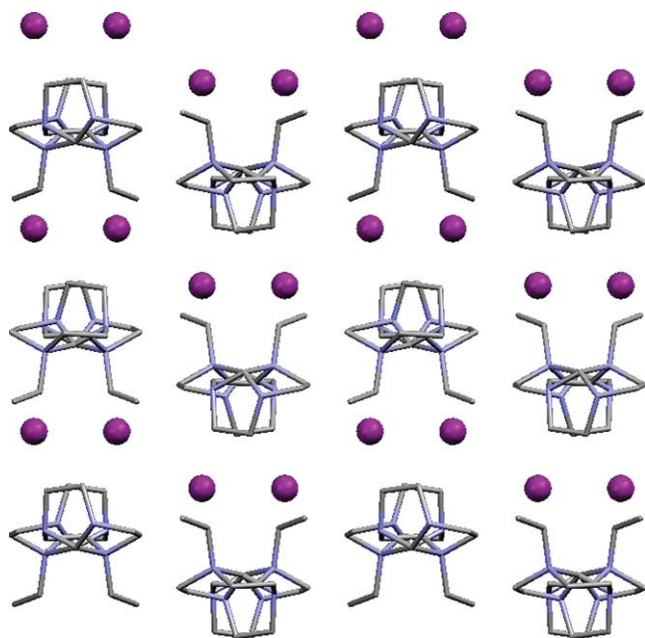


Figure 2. Mercury representation of the packing in **2**.

(Fig. 1), the cations themselves forming channels within the crystal lattice (Fig. 2), with the space between them occupied by the iodide anions. Data refinement ($R=2.3\%$) was such that the hydrogen atoms were located in the difference map. Weak interactions occur in the structure, and the molecules are oriented so as to maximize the spacing between each layer, the ethyl chain on each cation being directed into the cavities between the iodide anions (Table 1).

Table 2 summarises the bond length and angles for **2** while Table 3 details close contacts between the iodide ion and cation unit below 3.2 \AA . Other contacts between cations units include $\text{N}(3)\cdots\text{H}(1)$ ($-x+1/2, +y+1/2, +z$) $2.663(1) \text{ \AA}$ and $\text{N}(2)\cdots\text{H}(11)$ ($x-1/2, -y+1/2, -z+1$) $2.668(1) \text{ \AA}$. The angles around the central methine bridge are an interesting feature, particularly that between $\text{H}(18)-\text{C}(7)-\text{N}(1)$ ($103(1)^\circ$), which is lower than the ideal tetrahedral angle. The closest contact between the methine group and $\text{I}(1)$ is 3.45 \AA ($x+0.5, -y+0.5, -z+1$) indicating that steric factors do not contribute to the deviation from tetrahedral geometry around this carbon.

Table 1. Crystal structure refinement data for **2–5**

	2	3	4	5
Formula	$\text{C}_9\text{H}_{18}\text{N}_3\text{I}$	$\text{C}_{10}\text{H}_{20}\text{N}_3\text{I}$	$\text{C}_{14}\text{H}_{20}\text{N}_3\text{Br}$	$\text{C}_{18}\text{H}_{23}\text{N}_4\text{O}_2\text{Br}$
Formula weight	295.16	309.19	310.24	407.31
Crystal system	Orthorhombic	Monoclinic	Orthorhombic	Monoclinic
Space group	<i>Pbca</i>	<i>P2₁/n</i>	<i>Pbca</i>	<i>P2₁/c</i>
<i>a</i> (Å)	12.254(3)	7.009(1)	9.865(2)	13.458(3)
<i>b</i> (Å)	12.678(3)	14.038(3)	9.286(2)	32.440(7)
<i>c</i> (Å)	14.789(3)	12.731(3)	29.966(6)	8.263(2)
Volume (Å ³)	2297.7(8)	1212.1(4)	2745.0(10)	3572(13)
β (°)		104.61(3)		98.03(3)
ρ_c (g cm ⁻³)	1.707 ($Z=8$)	1.694 ($Z=4$)	1.501 ($Z=8$)	1.515 ($Z=8$)
μ_{Mo} (mm ⁻¹)	2.752	2.612	2.982	2.321
$T_{\text{min/max}}$	0.2169/0.8523	0.6953/0.9027	0.5599/0.8652	0.7370/0.9129
Reflections collected	15,782	9369	23,129	32,592
Independent reflections	2729 [$R_{\text{int}}=0.0459$]	2872 [$R_{\text{int}}=0.0824$]	3283 [$R_{\text{int}}=0.0787$]	8244 [$R_{\text{int}}=0.1266$]
<i>R</i>	0.023	0.0372	0.0372	0.0574
<i>R_w</i>	0.0392	0.0872	0.0853	0.1445

Table 2. Selected bond lengths (Å) and angles (°) in **2–5**

	2	3	4	5
N(1)–C(1)	1.505(3)	1.511(5)	1.511(3)	1.501(4)
N(1)–C(6)	1.504(3)	1.505(4)	1.494(3)	1.504(5)
N(1)–C(7)	1.658(3)	1.638(4)	1.661(3)	1.700(5)
N(1)–C(8)	1.509(3)	1.508(4)	1.513(3)	1.496(4)
N(2)–C(2)	1.476(3)	1.474(5)	1.463(3)	1.465(5)
N(2)–C(3)	1.488(3)	1.478(5)	1.478(3)	1.487(5)
N(2)–C(7)	1.417(3)	1.428(5)	1.413(3)	1.410(5)
N(3)–C(4)	1.484(3)	1.494(4)	1.488(3)	1.491(5)
N(3)–C(5)	1.461(3)	1.468(4)	1.457(3)	1.455(5)
N(3)–C(7)	1.413(3)	1.421(5)	1.411(3)	1.402(5)
C(1)–C(2)	1.516(3)	1.518(5)	1.517(3)	1.531(6)
C(4)–C(3)	1.516(4)	1.514(6)	1.472(4)	1.501(6)
C(5)–C(6)	1.539(3)	1.541(5)	1.518(3)	1.542(6)
N(1)–C(1)–C(2)	103.6(2)	104.5(3)	103.8(2)	103.3(3)
N(1)–C(6)–C(5)	103.6(2)	103.1(3)	104.2(2)	103.8(3)
N(1)–C(8)–C(9)	114.3(2)	115.5(3)	115.2(2)	115.2(3)
N(2)–C(2)–C(1)	105.4(2)	105.1(3)	105.7(2)	105.6(3)
N(2)–C(3)–C(4)	105.9(2)	102.9(3)	106.8(2)	105.8(3)
N(2)–C(7)–N(1)	106.8(2)	105.9(3)	106.4(2)	105.5(3)
N(3)–C(4)–C(3)	104.2(2)	105.3(3)	106.4(2)	104.4(3)
N(3)–C(7)–N(1)	106.1(2)	107.1(3)	106.0(2)	105.4(3)
N(3)–C(7)–N(2)	110.7(2)	110.3(3)	111.0(2)	110.7(3)
N(3)–C(5)–C(6)	105.3(2)	105.8(3)	105.8(2)	105.2(3)
C(1)–N(1)–C(7)	101.9(2)	103.2(3)	102.0(2)	101.7(3)
C(1)–N(1)–C(8)	112.5(2)	112.6(3)	112.4(2)	112.8(3)
C(2)–N(2)–C(3)	115.7(2)	115.4(3)	115.8(2)	116.1(3)
C(5)–N(3)–C(4)	115.1(2)	115.3(3)	114.6(2)	116.1(3)
C(6)–N(1)–C(1)	116.9(2)	116.2(3)	116.0(2)	116.8(3)
C(6)–N(1)–C(7)	102.6(2)	102.1(3)	102.4(2)	101.4(3)
C(6)–N(1)–C(8)	112.6(2)	112.6(3)	113.9(2)	113.9(3)
C(7)–N(2)–C(2)	106.1(2)	105.1(3)	106.4(2)	107.0(3)
C(7)–N(2)–C(3)	106.9(2)	105.3(3)	106.8(2)	107.5(3)
C(7)–N(3)–C(4)	106.4(2)	106.1(3)	105.9(2)	106.9(3)
C(7)–N(3)–C(5)	105.1(2)	106.7(3)	106.2(2)	105.5(3)
C(8)–N(1)–C(7)	108.9(2)	108.9(3)	108.7(2)	108.2(3)

This deviation may be due, in part, to the effect imposed by the long N(1)–C(7) bond length of $1.658(3) \text{ \AA}$, and partial amidinium character imposed on N(2) and N(3), as evidenced by the shorter N(2)–C(7) and N(3)–C(7) bond lengths of $1.417(3)$ and $1.413(3) \text{ \AA}$, respectively, compared with the other N–C distances in the molecule, which are typically $1.48\text{--}1.51 \text{ \AA}$. Figure 2 shows a representation of the packing in the molecule revealing that the ethyl arms are pointed towards the cavities between the molecules and that the iodo anions occupy the spaces between the cations.

An ORTEP representation of the cation **3** is shown in

Table 3. Hydrogen bonding contacts in **2** and **4**

	2		4		
	X···H Distance (Å)	X···H–Y Angle (°)	X···H Distance (Å)	X···H–Y Angle (°)	
I(1)···H(2)–C(1) ^a	3.09	169.6	C(8)–H(8A)···Br(1) ^b	2.80	172.2
I(1)···H(7)–C(4) ^c	3.15	154.5	C(5)–H(5A)···Br(1) ^b	2.81	155.4
I(1)···H(13)–C(7) ^d	3.17	157.1	C(2)–H(2A)···Br(1) ^e	2.84	168.9
I(1)···H(3)–C(2) ^f	3.18	81.3	C(2)–H(2B)···Br(1) ^f	2.87	160.9
			C(4)–H(4A)···N(2) ^g	2.52	141.4

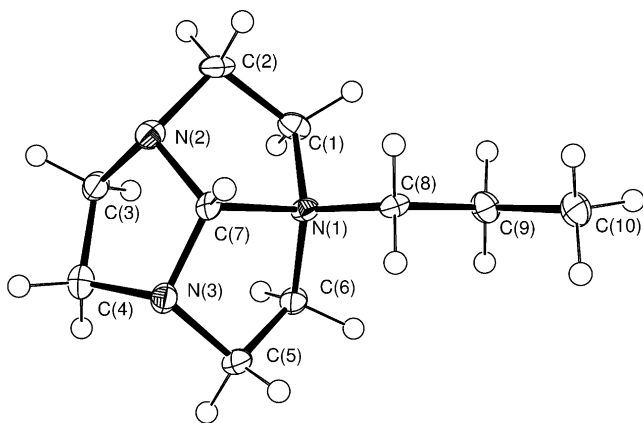
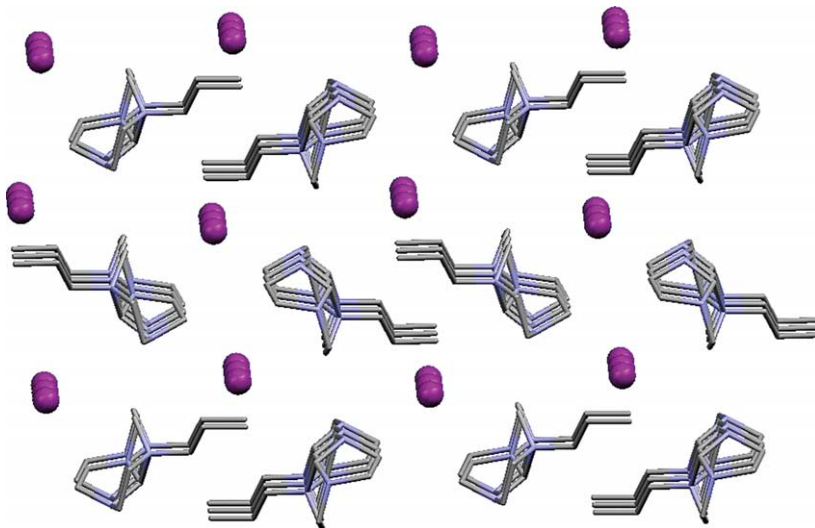
^a ($x+0.5, +y, -z+0.5$).^b ($x, +y+1, +z$).^c ($-x+1, +y-0.5, -z+0.5$).^d ($x+0.5, -y+0.5, -z+1$).^e ($-x+1.5, +y+0.5, +z$).^f ($-x+1, -y, -z+1$).^g ($x+0.5, +y, -z+0.5$).**Figure 3.** ORTEP representation of the cation in **3** (probability ellipsoids drawn at 50%).

Figure 3. The bond lengths and angles for the orthoamidinium ring are shown in Table 2. Again, this compound forms channels of cation and anion, the cation units being inverted in each column, so that the propyl chains of one row face those in the next row (i.e., in a head to head manner, Fig. 4), presumably in order to minimize contacts between neighbouring rings. The iodide anion sits almost equidistant between two propyl chains, the distance to the nearest hydrogen H(10C) (x, y, z) being 3.11 Å, while the

distance to the nearest (symmetry related) propyl chain is 3.05 Å (I(1)···H(10B) ($x+1, +y, +z$)). This atom position is almost perfectly equidistant from H(1A) of another symmetry related cation unit, the distance being also 3.05 Å (I(1)···H(1A) ($-x-0.5, +y+0.5, -z+0.5$)). Indeed, this contact may be representative of a weak hydrogen bond, the angle between C1–H(1A)···I(1) being 170.9°. The other closest contact occurs between N(3)···H(1B) ($x+1, +y, +z$), the distance being 2.78 Å. The propyl chain adopts the expected staggered conformation, the torsion angle between N(1)–C(8)–C(9)–C(10) being $-176.3(3)^\circ$.

The crystal structure of **4** is shown in Figure 5, the bond lengths and angles around the tacn orthoamidinium ring being detailed in Table 2. As is the case for the other compounds, the N(1)–C(7) distance is much longer than the other C(7)–N bonds, again indicating that this cation exhibits significant amidinium character. No π -stacking occurs in the molecules, the closest aromatic C···C interactions being around 4.1 Å. The cations stack in columns, each row of cations interspaced in a head to head manner, so that the aromatic rings are spaced perpendicular to each other (Fig. 6). The anion, in this instance bromide, occupies a cavity between neighbouring orthoamidinium rings. A hydrogen bonding network is present with the structure (Fig. 7) which is defined by close interactions between: (i) Br(1) and H(8B) ($-x+1.5,$

**Figure 4.** Mercury representation of the packing in **3**.

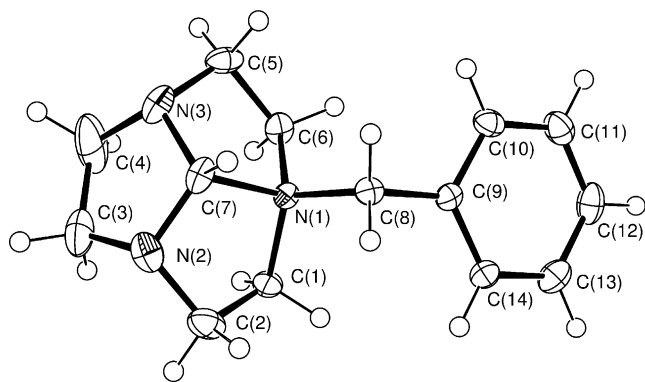


Figure 5. ORTEP representation of the cation **4** (probability ellipsoids drawn at 50%).

$+y+0.5, +z$) on the CH_2 bridge, $\text{Br}\cdots\text{H}$ distance 2.84 Å, and $\text{C}(8)\text{--H}(8\text{B})\cdots\text{Br}(1)$ angle 168.9°; (ii) $\text{H}(8\text{B})$ on the CH_2 bridge and a symmetry related bromide ion ($\text{H}(8\text{A})\text{Br}(1)$ ($x, +y+1, +z$; distance 2.80 Å); and (iii) a weak hydrogen bond between $\text{C}(4)\text{--H}(4\text{A})$ and $\text{N}(2)$ (distance 2.52 Å). The bromide also forms an interaction (2.87 Å) with $\text{H}(2\text{B})$ (tacn C–H) ($-x+1.5, +y+0.5, +z$) on the same cation.

Two molecules comprise the asymmetric unit in the crystal structure of **5**, an ORTEP representation of one being shown in Figure 8. The main difference between the two molecules arises primarily from the different twists of the phthalimido group about the propyl C–N bonds, as indicated by the torsion angles $\text{N}(\text{phth})\text{--C}(\text{a})\text{--C}(\text{b})\text{--C}(\text{c})$ (propyl) of -171.4° and 178.0° . Table 2 details selected bond lengths and angles around the orthoamidinium ring in one molecule. The orthoamidinium rings form rows, the spaces between the rings being once again occupied by the bromide anion. The molecules are oriented so that the phthalimide rings are arranged in a head to head fashion but do not stack directly above one another and so only form weak π -stacking interactions. Several hydrogen bonds are found in this structure and of particular note is the hydrogen bond occurring between $\text{C}(36)\cdots\text{H}(36)$ and $\text{O}(2)$ on the second cation in the asymmetric unit (distance 2.35 Å). A weaker intermolecular interaction occurs between $\text{C}(29)\text{--H}(29)$ and $\text{O}(4)$ on the same molecule (distance 2.53 Å). In the other

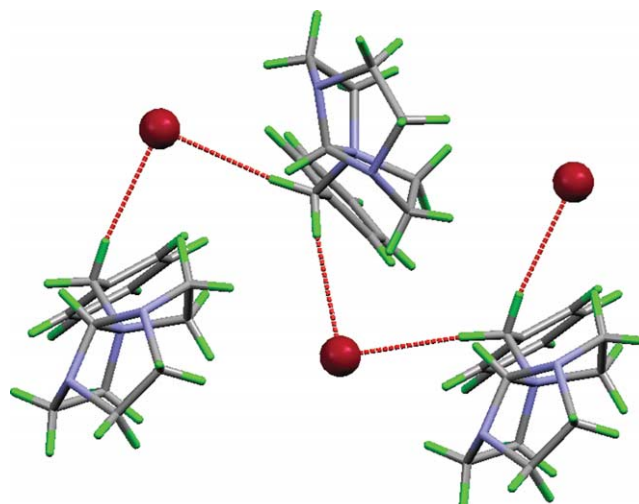


Figure 7. Mercury representation of the hydrogen-bonding network in **4**.

cation this interaction is weaker, the distance being 0.1 Å longer, as a consequence of a less acute twist of the phthalimide ring.

In summary, the structures of the amidinium salts presented herein exhibit long quaternary amine–methine carbon distances (1.64–1.70 Å) coupled with shorter methine–N bonds to the other nitrogen atoms (1.40–1.43 Å), which are indicative of double bond character within the $\text{N}(2)\text{--C}(7)\text{--N}(3)$ unit (see Table 4). Farrugia et al.³² have noted similar deviations in $\text{N}'\text{-(3-phenoxypropyl)4-7-diaza-1-azoniatricyclo[5.2.1.0}^{4,10}\text{]decane bromide hydrate}$. In contrast, in the crystal structure of triazatricyclo[5.2.1.0^{4,10}]decane, determined by Blake et al.³³ a symmetric conformation was observed, with an average methine–N distance of 1.474 Å.

2.2. Molecular modelling studies

Density functional calculations were undertaken on **2**, **4** and tacnoa using the crystal structures as the starting point for the optimizations. B3LYP optimization of **2** and **4** indicate that the low energy conformation is the amidinium ion in which the positive charge is delocalized over the two secondary amines instead of the tertiary amine $\text{N}(1)$ (Figs. 9

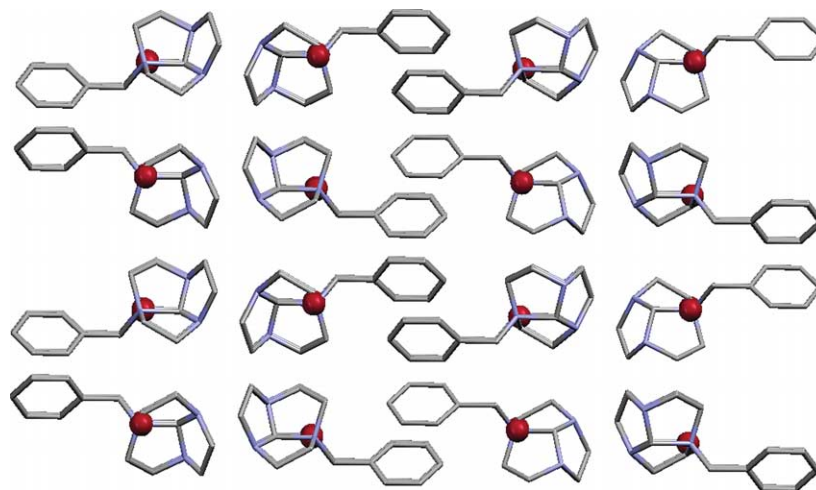


Figure 6. Mercury representation of the packing in **4**.

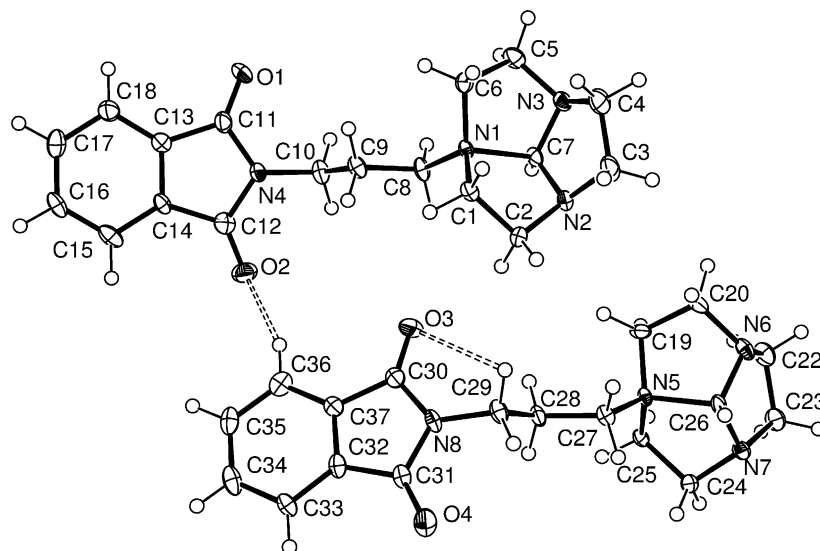


Figure 8. ORTEP representation of the cation **5** (probability ellipsoids drawn at 50%).

Table 4. C–N bond lengths (measured and calculated) for **2**, **4** and tacnoa

Bond	2		4		Tacnoa	
	Crystal (Å)	Model (Å)	Crystal (Å)	Model (Å)	Crystal (Å)	Model (Å)
N(1)–C(7)	1.658(3)	2.047	1.661(3)	1.803	1.472(3)	1.501
N(2)–C(7)	1.417(3)	1.366	1.413(3)	1.399	1.478(3)	1.469
N(3)–C(7)	1.418(3)	1.366	1.411(3)	1.395	1.473(3)	1.462

and **10**). This is highlighted by a shortening of the N(2)–C(7) and N(3)–C(7) distance in both compounds, and a longer N(1)–C(7) bond, which is the site of cleavage that ultimately forms the tertiary amine. The relevant bond distances are shown in Table 4. In order to determine the energy difference between the conformation found in the crystal structure and energy minimized structure, a minimization was performed in which the C–N bonds on the rings were constrained at their crystal structure values and this was then compared to the energy of structures determined without constraint. In each case, the lower energy amidinium conformations were found to be only

slightly more stable than the other but the energy differences were quite small, 2.4 and 1.9 kJ mol⁻¹ for the ethyl and benzyl derivatives, respectively. This means that minor crystal packing or solvation effects could easily result in a change in the preferred conformation in the solid state or solution.

By comparison, the energy minimized model of triaza-tricyclo[5.2.1.0^{4,10}]decane³³ is in good agreement with the crystal structure in bond lengths (Table 4), with an even atomic charge distribution over all three nitrogen atoms, all three atoms having a near neutral charge. Very little bond length or conformational changes occur in the other bonds, indicating that the charge and the methine bridge itself accounts for the instability of the amidinium salts. In both compounds the DFT calculations predicted that the positive charge on the tertiary N(1) migrates to N(2) and N(3). While

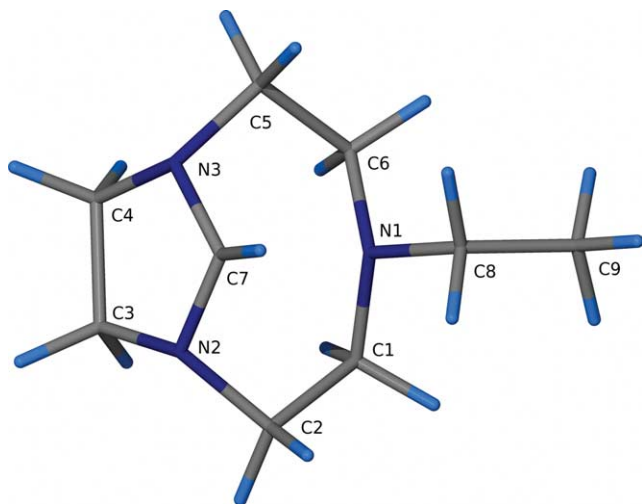


Figure 9. POV-Ray representation of the energy minimized structure of compound **2**.

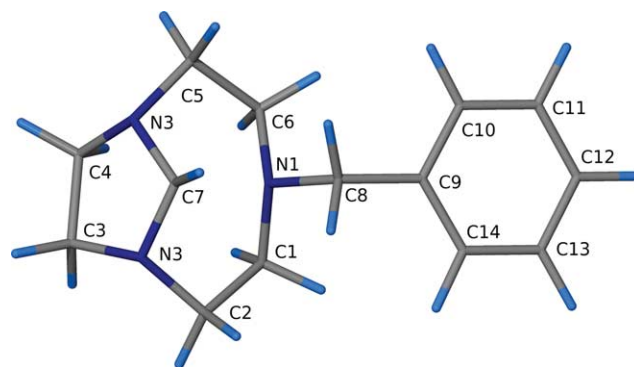


Figure 10. POV-Ray representation of the energy minimized structure of compound **4**.

this is feasible, it is likely that this charge is distributed over the N(2)–C(7)–N(3) bond, facilitating nucleophilic attack of the methine carbon by water.

A noteworthy feature of these systems is the difference in electron density on the CH₂ of the appended ethyl and benzyl groups. For the benzyl derivative, the energy minimized model shows a large negative atomic charge on C(8), while in the ethyl derivative this charge is typical of sp³ hybridised carbon alkyl chains. This increase in negativity on the benzyl derivative is supported by both experimental and crystallographic evidence. The crystal structure of **4** shows hydrogen bonding between the C(8) and two adjacent bromine molecules. Conversely, the three other crystal structures do not show the halide anions participating in hydrogen bonding with the equivalent CH₂ groups. We have also found (unpublished data) that benzyl derivatives of tacn undergo some cleavage of the benzyl group in acidic solution with up to 10% loss being observed. No such loss was noted for the corresponding ethyl or propyl derivatives.

2.3. Kinetic studies

The hydrolysis of tacnorthoamide and two amidinium derivatives, tacnoet (**2**) and tacnobz (**4**) to the corresponding formyl derivatives, 1-formyl-1,4,7-triazacyclononane, 1-ethyl-4-formyl-1,4,7-triazacyclononane and 1-benzyl-4-formyl-1,4,7-triazacyclononane was followed at 80 °C by ¹H NMR spectroscopy and rates of hydrolysis determined as described in Section 3. This experiment revealed that the non-ionic tacnorthoamide does not hydrolyse under the conditions used whilst compounds **2** and **4** do hydrolyse. Moreover, the rate of hydrolysis of **4** ($k = 6.28(\pm 0.20) \times 10^{-5} \text{ s}^{-1}$) was found to be 60 times faster than that measured for **2** ($k = 1.10(\pm 0.03) \times 10^{-6} \text{ s}^{-1}$). The slower rate of hydrolysis of tacnoa is not unexpected given the absence of a long N–C (methine) in this molecule (all bonds 1.474(3) Å) whilst in **2** and **4**, the C(methine)–N(quaternary) is much longer (1.660(3) Å) than the other bonds (1.41–1.42 Å). A difference in ground state stability could account for the difference in reaction rates observed for **2** and **4**. However, as the bond distances in **2** and **4**, determined by X-ray structure analysis, were identical it would be anticipated that the two amidinium salts would hydrolyse at the same rate. The conformation of the amidinium ion may be an important determinant of the relative rates of hydrolysis. As described above, molecular modelling calculations show a preference for this form, in which the positive charge is delocalized over the atoms N(2), C(7) and N(3). The effect this charge delocalisation has on the puckering of the three five membered rings is shown in Table 5, which details the RMS deviation from the least squares plane defined by those rings. The ring defined by N(3)–C(7)–N(2)–C(3)–C(4) shows the least deviation from the plane in both **2** and **4** but no such flattening of this ring is seen in the tacnorthoamide structure. Indeed, deviation of the plane by all three rings in this structure is almost uniform. In the case of **2** and **4**, the latter shows least deviation from the plane, and hydrolyses 60 times faster than **2**, while under the above conditions there is no noted hydrolysis of the non-ionic tacnorthoamide. It can therefore be argued that the flatter conformation in **4** is indicative of

Table 5. RMS deviation from the least squares planes in **2**, **4** and tacnoa

Compound	Ring	Deviation (Å)
Ethyl (2)	N(3)–C(7)–N(2)–C(3)–C(4)	0.1003
	N(1)–C(1)–C(2)–N(2)–C(7)	0.1703
	N(3)–C(5)–C(6)–N(1)–C(7)	0.1748
Benzyl (4)	N(3)–C(7)–N(2)–C(3)–C(4)	0.0723
	N(1)–C(1)–C(2)–N(2)–C(7)	0.1644
	N(3)–C(5)–C(6)–N(1)–C(7)	0.1660
Tacnorthoamide	N(3)–C(7)–N(2)–C(3)–C(4)	0.1542
	N(1)–C(1)–C(2)–N(2)–C(7)	0.1523
	N(3)–C(5)–C(6)–N(1)–C(7)	0.1523

more amidinium ion character than in **2** and that this contributes to faster nucleophilic attack at C(7) by water and hence a higher hydrolysis rate.

3. Experimental

3.1. Materials

Reagents and solvents were obtained from commercial suppliers and used without further purification. Distilled water was used throughout and acetonitrile was pre-dried over sieves prior to use. 1,4,7-Triazacyclonane trihydrochloride was prepared by the Richman–Atkins method.³⁴ Triazatricyclo[5.2.1.0^{4,10}]decane was synthesized according to a published method.²¹

3.2. Instrumentation

¹H and ¹³C NMR spectra were recorded on a Varian Mercury AM300 300 MHz spectrometer. The chemical shifts, δ , are reported in ppm (parts per million) using the high frequency positive convention, relative to an internal standard of tetramethylsilane (TMS) for non-aqueous solvents and sodium (2,2,3,3-d₄-3-(trimethylsilyl)propionate (TMSP-D) for D₂O. Microanalyses were performed by the Campbell Microanalytical Laboratory, University of Otago, New Zealand. Mass spectra were obtained using a Micromass Platform Quadrupole Mass Spectrometer fitted with an electrospray source.

3.3. Preparation of amidinium compounds

Compounds **1** and **2**,³¹ **4**⁴ and **5**⁷ have been reported previously. In this study, however, these and compound **3** were prepared using the procedure described below for 1-methyl-4,7-diaza-1-azoniatricyclo[5.2.1.0^{4,10}]decane iodide (**1**). Typically triazatricyclo[5.2.1.0^{4,10}]decane (0.41 g, 2.9 mmol) was dissolved in 10 mL MeCN and the solution was stirred. To this solution was added iodomethane (0.489 g, 3.45 mmol) in 5 mL MeCN and the solution was stirred at room temperature. A white solid slowly formed, and the solution was allowed to stir at room temperature for 18 h. The white solid was collected by vacuum filtration, and washed with ether and air dried, the filtrate producing more precipitate on washing with ether. This solid was also collected by filtration and was found to be of equal purity to the first crop of product.

3.3.1. 1-Methyl-4,7-diaza-1-azoniatricyclo[5.2.1.0^{4,10}]decane (1**).** Yield, 0.72 g, 90%. Anal. Calcd for 1·1/2H₂O

(C₈H₁₇N₃O_{1/2}I): C 33.1, H 5.9, N 14.5%. Found: C 32.7, H 5.9, N 14.2%. NMR spectra (*d*₃-MeCN): ¹H δ 5.43 (s, 1H, CH bridge), 3.72–3.47 (m, 8H, CH₂ ring), 3.25–3.15 (m, 4H, CH₂ ring), 3.11 (s, 3H, NCH₃); ¹³C δ 126.3, (1C, CH bridge), 61.74, (2C, CH₂N(Me)CH₂), 57.40 (2C, CH₂ ring), 53.21 (2C, CH₂ ring), 48.53 (1C, NCH₃). ESI mass spectrum (MeCN): M⁺ 154.2.

3.3.2. 1-Ethyl-4,7-diaza-1-azoniatricyclo[5.2.1.0^{4,10}]decane (2). Yield, 95%. Anal. Calcd for C₉H₁₈N₃I: C 36.6, H 6.2, N 14.2%. Found: C 36.7, H 6.0, N 14.5%. NMR spectra (*d*₃-MeCN): ¹H, δ 5.58 (s, 1H, CH bridge), 3.70 (m, 3H, CH₂ tacn ring), 3.46 (m, 4H, NCH₂CH₃ and CH₂ tacn ring), 3.24 (m, 4H CH₂ tacn ring), 1.48 (t, 3H, NCH₂CH₃); ¹³C δ 142.2 (1C, CH bridge), 57.5 (2C, CH₂ tacn ring), 56.5 (2C, CH₂ tacn ring), 54.3 (1C, NCH₂CH₃), 52.6 (2C, CH₂ tacn ring), 10.6 (1C, NCH₂CH₃). ESI mass spectrum (MeCN): M⁺ 168.2. Crystals for X-ray crystallography were grown by vapour diffusion of ether into a MeCN solution of **2**.

3.3.3. 1-*n*-Propyl-4,7-diaza-1-azoniatricyclo[5.2.1.0^{4,10}]decane (3). Yield, 95%. Anal. Calcd for C₁₀H₂₀N₃I: C 38.9, H 6.5, N 13.6%. Found: C 39.1, H 6.5, N 13.6%. NMR Spectra (*d*₃-MeCN): ¹H, δ 5.49 (s, 1H, CH bridge), 3.67–3.57 (m, 6H, CH₂ tacn ring), 3.42–3.12 (m, 8H, 6H from CH₂ tacn ring and 2H NCH₂CH₂CH₃), 1.87–1.76, (sextet, 2H, NCH₂CH₂CH₃), 0.97, (t, 3H, NCH₂CH₂CH₃); ¹³C δ 124.9, (1C, CH bridge), 60.53, (1C, NCH₂CH₂CH₃), 58.07 (2C, CH₂ tacn ring), 56.70, (2C, CH₂ tacn ring), 52.70 (2C, CH₂ tacn ring), 18.97 (1C, NCH₂CH₂CH₃), 11.00 (1C, NCH₂CH₂CH₃). ESI mass spectrum (MeCN): M⁺ 182.3. Crystals for X-ray crystallography were grown by vapour diffusion of ether into a MeCN solution of **3**.

3.3.4. 1-Benzyl-4,7-diaza-1-azoniatricyclo[5.2.1.0^{4,10}]decane (4). Yield, 92%. Anal. Calcd for 4·1/2H₂O (C₁₄H₂₁N₃O_{1/2}Br): C 52.7, H 6.6, N 13.2%. Found: C 52.3, H 6.4, N 13.1%. NMR spectra (*d*₃-MeCN): ¹H, δ 7.63–7.61 (m, 2H, CH ar), 7.51–7.49 (m, 3H, CH ar), 5.79, (s, 1H, CH bridge), 3.77–3.71 (m, 2H, NCH₂-C(ar)), 3.56–3.51 (m, 4H, CH₂ tacn ring), 3.30–3.10 (m, 8H CH₂ tacn ring); ¹³C δ 133.6, (2C CH(ar)), 131.7 (1C, CH(ar)), 131.1 (1C, C(ar)-CH₂), 130.7 (2C, CH(ar)), 125.62 (1C, CH bridge), 62.46 (1C, NCH₂-C(ar)), 58.37 (2C, CH₂ tacn ring), 57.26 (2C, CH₂ tacn ring), 53.16 (2C, CH₂ tacn ring). ESI mass spectrum (MeCN): M⁺ 230.3. Trace hydrolysis (~1%) of the compound occurred due to trace amounts of H₂O in the *d*₃-MeCN. Crystals for X-ray crystallography were grown by vapour diffusion of ether into a MeCN solution of **4**.

3.3.5. 1-Propylphthalimido-4,7-diaza-1-azoniatricyclo[5.2.1.0^{4,10}]decane (5). Yield, 93%. Anal. Calcd for 5·1/2H₂O (C₁₈H₂₄N₄O_{5/2}Br): C 51.9, H 5.8, N 13.5%. Found C 52.2, H 5.7, N 13.6%. NMR Spectra (*d*₃-MeCN): ¹H δ 7.84–7.78 (m, 4H, CH(ar)), 5.46 (s, 1H, CH bridge), 3.73 (t, 2H, NCH₂CH₂CH₂-phth), 3.63–3.51 (m, 6H CH₂ tacn ring), 3.31–3.08 (m, 8H, 6H from CH₂ tacn ring, and 2H from NCH₂CH₂CH₂-phth), (NCH₂CH₂CH₂-phth under H₂O peak), ¹³C δ 169.75 (2C, C=O), 135.72 (2C, CH(ar)), 133.69(2C, C(ar)) 127.05 (1C, CH bridge), 124.37 (2C, CH(ar)), 58.20 (2C, CH₂ tacn ring), 57.41 (2C, CH₂ tacn ring), 56.89 (1C, NCH₂CH₂CH₂-phth), 53.09 (2C, CH₂ tacn

ring), 36.29 (1C, NCH₂CH₂CH₂-phth), 25.59 (1C, NCH₂-CH₂CH₂-phth). ESI mass spectrum (MeCN): M⁺ 328.4. Crystals for X-ray crystallography were grown by vapour diffusion of ether into a MeCN solution of **5**.

3.4. X-ray crystallography

All structures were collected on an Enraf-Nonius CAD4 diffractometer with monochromated Mo K α radiation (λ = 0.71073 Å) at 123(2) K using phi and/or omega scans. Data were corrected for Lorentz and polarization effects and absorption corrections were applied. The structures were solved by the direct methods and refined using full matrix least-squares within the programs SHELXS-97 and SHELXL-97³⁵ respectively. The program X-Seed³⁶ was used as an interface to the SHELX³⁵ programs, and to prepare the figures. Crystallographic data (excluding structure factors) for the structures presented in this paper have been deposited with the Cambridge Crystallography Data Centre as supplementary publication numbers CCDC 258759–258762. Copies of the data can be obtained, free of charge, on application to CCDC, 12 Union Road, Cambridge CB2 1EZ [fax: +44 1223 336 033 or e-mail: deposit@ccdc.cam.ac.uk]. Crystal data for the compounds are given in Table 1.

3.5. Molecular modelling calculations

All theoretical calculations were carried out using Gaussian 98³⁷ running SuSe linux 9.1 on a Dell Optiplex 4700 PC. B3LYP optimisations^{38,39} using the 6-31G* basis^{40,41} were employed for both compounds.

3.6. Kinetic studies

The hydrolysis of tacnoa, tacnoaet (**2**) and tacnoabz (**4**) was studied in aqueous solution at pH ~7 using ¹H NMR spectroscopy. A 0.1 M solution of each compound was prepared by dissolving a sample of each compound in 5 mL of D₂O. The ¹H NMR spectrum of each solution was recorded immediately after preparation and then at various times after heating to 80 °C after quenching the reaction on ice. The fraction of each compound converted into the corresponding formyl derivative was determined from the ratio of the integration of the formyl proton signal on the product to that of the single methine proton on the reactant. In the case of tacnoa, there was little evidence of hydrolysis, after several days heating at 80 °C. For the other two compounds, the rate of conversion of starting materials to the formyl derivatives was obtained by fitting the variation in the fraction of formyl product formed with time to the simple exponential function, $F = m \exp(kt)$, where F is the fraction of reactant converted to formyl product, m is a pre-exponential term, k is the rate constant and t is the time elapsed.

Acknowledgements

Financial support from the Monash University and Australian Research Council through the Australian Centre for Nanostructured Electromaterials is gratefully

acknowledged. The authors wish to also thank Drs Evan Robinson and Siân Howard for assistance with Molecular Modeling.

References and notes

1. Atkins, T. J. *J. Am. Chem. Soc.* **1980**, *102*, 6364–6365.
2. Erhardt, J. M.; Grover, E. R.; West, J. D. *J. Am. Chem. Soc.* **1980**, *102*, 6365–6369.
3. Weisman, G. R.; Johnson, V. B.; Fiala, R. E. *Tetrahedron Lett.* **1980**, *21*, 3635–3638.
4. Weisman, G. R.; Vachon, D. J.; Johnson, V. B.; Gronbeck, D. A. *J. Chem. Soc., Chem. Commun.* **1987**, 886–887.
5. Alder, R. W.; Mowlam, R. W.; Vachon, D. J.; Weisman, G. R. *J. Chem. Soc., Chem. Commun.* **1992**, 507–508.
6. Blake, A. J.; Fallis, I. A.; Parsons, S.; Ross, S. A.; Schröder, M. *J. Chem. Soc., Dalton Trans.* **1996**, 525–532.
7. Warden, A. C.; Graham, B.; Hearn, M. T. W.; Spiccia, L. *Org. Lett.* **2001**, *3*, 2855–2858.
8. McGowan, P. C.; Podesta, T. J.; Thornton-Pet, M. *Inorg. Chem.* **2001**, *40*, 1445–1453.
9. Long, N. J.; Parker, D. G.; Speyer, P. R.; White, A. J. P.; Williams, D. J. *J. Chem. Soc., Dalton Trans.* **2002**, 2142–2150.
10. Haines, R. I. *Rev. Inorg. Chem.* **2001**, *21*, 165–205.
11. Farrugia, L. J.; Lovatt, P. A.; Peacock, R. D. *Inorg. Chim. Acta* **1996**, *246*, 343–348.
12. Ellis, D.; Farrugia, L. J.; Peacock, R. D. *Polyhedron* **1999**, *18*, 1229–1234.
13. Kovacs, Z.; Sherry, A. D. *Tetrahedron Lett.* **1995**, *36*, 9269–9272.
14. Stockheim, C.; Hoster, L.; Weyhermuller, T.; Wieghardt, K.; Nuber, B. *J. Chem. Soc., Dalton Trans.* **1996**, 4409–4416.
15. Schulz, D.; Weyhermuller, T.; Wieghardt, K.; Nuber, B. *Inorg. Chim. Acta* **1995**, *240*, 217–229.
16. Blake, A. J.; Champness, N. R.; Chung, S. S. M.; Li, W. S.; Schröder, M. *Chem. Commun.* **1997**, 1675–1676.
17. Blake, A. J.; Fallis, I. A.; Heppeler, A.; Parsons, S.; Rose, S. A.; Schröder, M. *J. Chem. Soc., Dalton Trans.* **1996**, 31–43.
18. Blake, A. J.; Fallis, I. A.; Gould, R. O.; Parsons, S.; Ross, S. A.; Schröder, M. *J. Chem. Soc., Dalton Trans.* **1996**, 4379–4387.
19. Graham, B.; Fallon, G. D.; Hearn, M. T. W.; Hockless, D. C. R.; Lazarev, G.; Spiccia, L. *Inorg. Chem.* **1997**, *36*, 6366–6373.
20. Spiccia, L.; Graham, B.; Hearn, M. T. W.; Lazarev, G.; Moubaraki, B.; Murray, K. S.; Tiekink, E. R. T. *J. Chem. Soc., Dalton Trans.* **1997**, 4089–4098.
21. Zhang, X.; Hsieh, W.-Y.; Margulis, T. N.; Zompa, L. J. *Inorg. Chem.* **1995**, *34*, 2883–2888.
22. Graham, B.; Grannas, M. J.; Hearn, M. T. W.; Kepert, C. M.; Spiccia, L.; Skelton, B. W.; White, A. H. *Inorg. Chem.* **2000**, *39*, 1092–1099.
23. Graham, B.; Spiccia, L.; Fallon, G. D.; Hearn, M. T. W.; Mabbs, F. E.; Moubaraki, B.; Murray, K. S. *J. Chem. Soc., Dalton Trans.* **2002**, 1226–1232.
24. Graham, B.; Hearn, M. T. W.; Junk, P. C.; Kepert, C. M.; Mabbs, F. E.; Moubaraki, B.; Murray, K. S.; Spiccia, L. *Inorg. Chem.* **2001**, *40*, 1536–1543.
25. Graham, B.; Spiccia, L.; Fallon, G. D.; Hearn, M. T. W.; Mabbs, F. E.; Moubaraki, B.; Murray, K. S. *J. Chem. Soc., Dalton Trans.* **2001**, 1226–1232.
26. Bond, A. M.; Graham, B.; Hearn, M. T. W.; Kepert, C. M.; Spiccia, L. *J. Chem. Soc., Dalton Trans.* **2001**, 2232–2238.
27. Graham, B.; Fallon, G. D.; Hearn, M. T. W.; Spiccia, L.; Moubaraki, B.; Murray, K. S. *J. Chem. Soc., Dalton Trans.* **2002**, 1226–1232.
28. Farrugia, L. J.; Lovatt, P. A.; Peacock, R. D. *J. Chem. Soc., Dalton Trans.* **1997**, 911–912.
29. DasGupta, B.; Katz, C.; Israel, T.; Watson, M.; Zompa, L. J. *Inorg. Chim. Acta* **1999**, *292*, 172–181.
30. Haidar, R.; Ipek, M.; DasGupta, B.; Yousaf, M.; Zompa, L. J. *Inorg. Chem.* **1997**, *36*, 3125–3132.
31. Koek, J. H.; Russell, S. W.; Wolf, L. v. d.; Hage, R.; Warnaar, J. B.; Spek, A. L.; Kerschner, J.; DelPizzo, L. *J. Chem. Soc., Dalton Trans.* **1996**, 353–362.
32. Farrugia, L. J.; Lovatt, P. A.; Peacock, R. D. *Acta Crystallogr. C* **1993**, *C49*, 2161–2164.
33. Blake, A. J.; Fallis, I. A.; Gould, R. O.; Harris, S. G.; Parsons, S.; Ross, S. A.; Schröder, M. *Acta Crystallogr. C* **1995**, *C51*, 738–741.
34. Richman, J. E.; Atkins, T. J. *J. Am. Chem. Soc.* **1974**, *96*, 2268–2270.
35. Sheldrick, G. M. *SHELXS97 and SHELXL97*, 1997.
36. Barbour, L. J. *J. Supramolecular Chem.* **2001**, *1*, 189.
37. Frisch, M. J.; Trucks, G. W.; Schlegel, H. B.; Scuseria, G. E.; Robb, M. A.; Cheeseman, J. R.; Zakrzewski, V. G.; Montgomery, J. A., Jr.; Stratmann, R. E.; Burant, J. C.; Dapprich, S.; Millam, J. M.; Daniels, A. D.; Kudin, K. N.; Strain, M. C.; Farkas, O.; Tomasi, J.; Barone, V.; Cossi, M.; Cammi, R.; Mennucci, B.; Pomelli, C.; Adamo, C.; Clifford, S.; Ochterski, J.; Petersson, G. A.; Ayala, P. Y.; Cui, Q.; Morokuma, K.; Malick, D. K.; Rabuck, A. D.; Raghavachari, K.; Foresman, J. B.; Cioslowski, J.; Ortiz, J. V.; Baboul, A. G.; Stefanov, B. B.; Liu, G.; Liashenko, A.; Komaromi, P. P.; Gomperts, R.; Martin, R. L.; Fox, D. J.; Keith, T.; Al-Laham, M. A.; Peng, C. Y.; Nanayakkara, A.; Challacombe, M.; Gill, P. M. W.; Johnson, B.; Chen, W.; Wong, M. W.; Andres, J. L.; Gonzalez, C.; Head-Gordon, M.; Replogle, E. S.; Pople, J. A. *Gaussian 98 Revision A9*; Gaussian, Inc., Pittsburgh, PA, 1998.
38. Becke, A. D. *J. Chem. Phys.* **1993**, *98*, 5648–5652.
39. Lee, C.; Yang, W.; Parr, R. G. *Phys. Rev. B* **1988**, *37*, 785–789.
40. Ditchfield, R.; Hehre, W. J.; Pople, J. A. *J. Chem. Phys.* **1971**, *54*, 724–728.
41. Clark, T.; Chandrasekhar, J.; Spitznagel, G. W.; Schleyer, P. v. R. *J. Comput. Chem.* **1983**, *4*, 294–301.